Core−Shell Cylinder Morphology in Poly(styrene-*b*-1,3-cyclohexadiene) Diblock Copolymers

Jennifer L. David and Samuel P. Gido*

Department of Polymer Science and Engineering, University of Massachusetts at Amherst, Amherst, Massachusetts 01003

Kunlun Hong, Jian Zhou, and Jimmy W. Mays

Department of Chemistry, University of Alabama at Birmingham, Birmingham, Alabama 35294

Nora Beck Tan

Polymers Research Branch, U.S. Army Research Laboratory, APG, Maryland 21005-5069

Received July 8, 1998; Revised Manuscript Received January 28, 1999

ABSTRACT: A microphase-separated core−shell cylinder morphology has been observed, via transmission electron microscopy and small-angle X-ray scattering, in diblock copolymers of polystyrene (PS) and poly(1,3-cyclohexadiene) (PCHD). The structures consist of PS cylindrical cores surrounded by PCHD cylindrical annuli which are then hexagonally packed in a matrix of PS. The materials were produced by anionic polymerization of styrene followed by 1,3-cyclohexadiene. Characterization by size exclusion chromatography revealed a main peak due to diblock with a very narrow molecular weight distribution. However, a significant amount of PS homopolymer (about 30%) was present in the as-synthesized materials. The as-synthesized materials with homopolymer present produced core−shell morphologies, and these structures became much more regular when the homopolymer was removed by fractionation. After fractionation, the pure core−shell forming diblocks had PCHD volume fractions of around 0.37 and polydispersities well under 1.1.

Introduction

The rich nature of microphase separation behavior in block copolymer systems is constantly reaffirmed as new morphologies continue to be discovered and characterized. The classical block copolymer morphologies (spheres, cylinders, and lamella) have been known since the 1960s. Beginning in the middle 1980s the discovery of exotic new morphologies such as cubic bicontinuous structures,[1−6] and perforated lamellar structures[7−10] has provided new challenges to our understanding of microphase separation in these materials. Recent work[11−15] on ABC triblock systems has begun to reveal a whole host of even more complex microphase separated structures.

Core−shell microphase-separated structures involving concentric layers with cylindrical geometry have been postulated but rarely observed experimentally. Specifically, core−shell structures have not been seen in diblock copolymers, although a core−shell cylinder morphology was theoretically predicted[16] for blends of diblock copolymers A−B_1 and A−B_2, where the A block was the same length for both copolymers. To date, this theoretical prediction has not been experimentally confirmed. Core−shell cylinder structures have been observed in linear triblock copolymers of poly(2-vinylpyridine) (33 vol %), polyisoprene (33 vol %), and polystyrene (33 vol %).[17] In this structure a cylindrical core of poly(2-vinylpyridine) is surrounded by a cylindrical annulus of polyisoprene, which is surrounded by a matrix of polystyrene. Both Noda[11] and Stadler[13] have also reported structures in ABC triblocks which have some aspects of core−shell structure. Nanometer scale core−shell spherical particles of poly(tetrafluoroethylene) and poly(methyl methacrylate) have also recently been produced by emulsion polymerization in CO_2.[18] This route to core−shell structures is fundamentally different, however, since it involves assembly of core shell structures through processing rather than self-assembly based on the molecular structure.

In the current paper, we describe the anionic synthesis of diblock copolymers of polystyrene and polycyclohexadiene, and we present transmission electron microscopy (TEM) and small-angle X-ray scattering (SAXS) results on these materials. Together, these techniques have enabled the clear identification of core−shell cylindrical structures. Although the phase separation behavior of PS−PCHD diblock copolymers (higher 1,2-content in the PCHD blocks than our materials) with nearly equal volume fractions has been recently investigated,[19] to date there has been no study of the morphology in other regions of the morphology diagram. Unlike the lamellar structure observed in that prior work, the core−shell cylinder structure described here represents what appears to be a unique morphology.

Experimental Section

Synthesis. All reagents and chemicals were purchased from Aldrich. Styrene was purified on the vacuum line by exposure to CaH_2 (24 h) and then dibutylmagnesium (12 h) with rigorous degassing. 1,3-Cyclohexadiene was purified by exposure to CaH_2, Na dispersion, and n-BuLi (30 min at 0 °C) on the vacuum line. The methanol used for termination of the reaction was degassed on a vacuum line. The benzene and hexane solvents were treated with concentrated sulfuric acid for at least 2 weeks to remove olefinic impurities. The solvents were then purified by exposure to CaH_2, Na dispersion, and poly(styryllithium) with rigorous degassing.

* To whom correspondence should be addressed.

10.1021/ma9810722 CCC: $18.00
Published on Web 04/21/1999

Chart 1

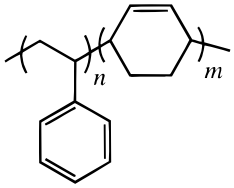

Poly(styrene-*b*-1,3-cyclohexadiene) diblock copolymers (Chart 1) were synthesized via anionic polymerization of styrene followed by cyclohexadiene.

A glass reaction apparatus was first prepared consisting of a main reaction bulb and, attached to it by means of a glass constriction, five smaller ampules with break seals. A mixture of benzene and hexane (in a ratio of 60:40 by volume), was vacuum distilled into the main bulb, and the four ampules were charged with *sec*-BuLi, styrene, cyclohexadiene, and methanol. The fifth ampule was reserved for sampling the molecular weight of the polystyrene, prior to addition of cyclohexadiene monomer. Polymerization of styrene was achieved by addition of *sec*-BuLi and styrene to the reaction bulb and stirring at room temperature. An orange-red color, characteristic of the living styryl anion, was observed immediately upon mixing of the monomer and initiator and persisted throughout the styrene polymerization. After 24 h, an aliquot of the reaction mixture was removed by tilting the apparatus such that a small amount of the polymer solution was collected into the fifth ampule. This sampling ampule was then sealed off from the main apparatus, and the main bulb was charged with cyclohexadiene monomer and immediately immersed in a −12 °C constant-temperature bath. The color of the reaction mixture was observed to change from orange-red to light yellow once the cyclohexadiene addition occurred. The slow kinetics and low temperature of the cyclohexadiene polymerization required a lengthy reaction time of 6−30 days, depending upon the molecular weight of polycyclohexadiene desired. Once the target reaction time was reached, polymerizations were terminated using the methanol sealed in the attached, fourth ampule. Polymer was recovered by precipitation in large amounts of methanol which contained the antioxidant BHT.

Molecular Characterization. The number average (M_n) and weight average (M_w) molecular weights of the diblock copolymers, prepared as described above, were determined using a Perseptive Biosystems Voyager Elite DE matrix-assisted laser desorption/ionization time-of-flight mass spectrometer (MALDI−TOF−MS) in linear mode. THF and indole acrylic acid (IAA) were used as solvent and salt, respectively. M_n was also measured using a Jupiter 230 membrane osmometer with toluene as the solvent. Table 1 lists the characteristics of the diblock copolymers used in this study, each with a different weight percent of polycyclohexadiene. The weight percent of polycyclohexadiene was calculated by integration of the appropriate peaks in the ^{1}H NMR spectra of the samples. These spectra were collected using a Bruker AMX 600 MHz NMR with $CDCl_3$ as the solvent. The major microstructure in the PCHD blocks consists of 1,4-units (>85%), as revealed by 2D NMR. Subsequent fractionation (by successive precipitation from a mixed toluene/methanol system) removed polystyrene and polycyclohexadiene homopolymers, and the resultant "true" weight percents of the pure diblocks were determined similarly. From these values, the volume fractions were calculated using the respective densities. (Polystyrene has a density of 1.05 g/mL, and the density of polycyclohexadiene, estimated by submersing solid pieces of a cast, dried, homopolymer film in sodium chloride solutions of various densities, was found to be 1.10 ± 0.05 g/mL.) As can be seen from Table 1, the majority component in each of these samples is polystyrene. Attempts to synthesize a diblock with a majority polycyclohexadiene component were not successful with the chosen initiator and solvent system because, above about 39 wt % polycyclohexadiene, the diblock precipitates from the reaction mixture. As a result, the volume fraction range available for these systems was limited. This study focuses on the morphology for three of the prepared samples (PS−PCHD-1, PS−PCHD-2, and PS−PCHD-3), as well as their fractionated products. We are currently examining several other diblocks with lower percent polycyclohexadiene. A comparison of the ^{1}H NMR spectrum before and after fractionation shows that the amount of homopolymer contamination in the as-synthesized PS−PCHD-1 and PS−PCHD-3 samples was approximately 30 wt %. (There was not a sufficient amount of PS−PCHD-2 polymer to fractionate.) ^{1}H NMR of the recovered homopolymer fraction shows that small amounts of cyclohexadiene residues are present in addition to styrene residues, the majority component (Table 1). Thus, the fractionation procedure removes the main PS homopolymer contaminant along with a small fraction of the diblock and/or residual, low molecular weight PCHD homopolymer. Any low molecular weight homopolymer results from a well-known chain transfer to monomer process inherent in cyclohexadiene polymerizations in hydrocarbon solvents.[20]

Table 1. Molecular Characteristics

sample	wt % PCHD[a]	ϕ of PCHD[b]	M_n[c]	M_n[d]	M_w/M_n[c]	M_w/M_n[d]
PS−PCHD-1	35.4	0.34	24 000	22 500	1.27	1.06
fract PS−PCHD-1	38.6	0.37		23 000		1.01
PS−PCHD-2	32.9	0.32	37 000	37 300	1.14	1.05
PS−PCHD-3	30.7	0.30	39 000	37 000	1.08	1.07
fract PS−PCHD-3	38.7	0.38		37 300		1.02

[a] By integration of 600 MHz ^{1}H NMR spectrum. [b] Calculated utilizing ρ(PS) = 1.05 g/mL^3 at 25 °C and ρ(PCHD) = 1.10 g/mL^3 at 25 °C along with the wt % data from ^{1}H NMR. [c] By membrane osmometry. [d] By MALDI−TOF.

Table 2. Solubility Parameters[a]

	PS	PCHD	cyclo-hexane	tolu-ene	tetra-hydrofuran	diox-ane
tablulated δ[b]	18.5		16.7	18.3	19.5	20.3
calculated δ[c]	19.3	18.2	16.8	17.7	19.7	19.9
$\Delta\delta$ of PS[d]		1.1	2.5	1.6	0.4	0.6
$\Delta\delta$ of PCHD[d]	1.1		1.4	0.5	1.5	1.7

[a] All solubility parameter values in this table are given in units of MPa$^{1/2}$. [b] Tabulated in ref 21. [c] Calculated using the group molar attraction constants tabulated in ref 23 (specifically the values adapted from Hoy). [d] Determined by taking the difference between the calculated solubility parameter for the indicated polymer and the polymer or solvent in each respective column.

Morphological Characterization. Solid sample films, approximately 1 mm in thickness, were obtained by casting the as-synthesized and fractionated polymer samples from a variety of solvents. The solvents (toluene, cyclohexane, THF, and dioxane) were chosen such that an entire range of selectivity for the two blocks was represented. Although we have not yet measured the second virial coefficient, A_2, directly for PCHD in these solvents, the relative solubilities were estimated though calculations of the Hildebrand solubility parameter (δ). Much has been published over the last 50 years on the use of group molar attraction constants to determine solubility parameters for both small molecules and polymers.[21−25] Table 2 reveals that, of our four solvents, two show pronounced selectivity for the PCHD block (cyclohexane and toluene) and two are selective for PS (THF and dioxane). The solvents in Table 2 are listed in approximate order of decreasing selectivity for PCHD and increasing selectivity for PS. As shown in Table 2, this is accomplished by comparing the absolute differences between the solubility parameters of the polymer and the solvent ($\Delta\delta = |\delta_P - \delta_S|$).

Total solvent casting times exceeded 14 days in all cases, at which point the samples were placed under vacuum at room temperature for several days to remove residual solvent. At this point each specimen was divided, one part being used for TEM and SAXS analysis of the as cast and unannealed morphology. The other part of each specimen was then thermally annealed in the melt. For annealing, samples were

Table 3. Morphological Summary[a]

	PS−PCHD-1			PS−PCHD-2		PS−PCHD-3		
solvent	cast	ann	fract	cast	ann	cast	ann	fract
cyclohexane	S*	CS*	D	(cs)	(cs)	S	CS*	CS*
toluene	CS*	CS	D	CS	CS	(cs)	(cs)	CS*
tetrahydrofuran	CS	CS	CS*	CS	CS	(cs)	(cs)	(cs)
dioxane	D	D	CS	CS	(cs)	D	D	D

[a] Key: CS* = extememly well-ordered core−shell cylinder morphology; CS = ordered core−shell cylinder morphology; (cs) = beginnings of core−shell morphology; S* = extremely well-ordered solid cylinder morphology; S = ordered solid cylinder morphology; D = disordered.

then placed in glass ampules. Precautions were taken to remove trace amounts of air from the environment by flushing with N_2 three times before sealing under a vacuum. The ampules were placed in a vacuum oven and heated to 120 °C, a temperature which is above the glass transition temperatures (T_g) for both PS and PCHD. The samples were held at this final annealing temperature for over 1 week and then allowed to cool to ambient temperature. Some samples were quenched directly from the 120 °C melt into liquid nitrogen. However, no difference in morphology was observed between samples which were allowed to cool slowly from 120 °C and those which were rapidly quenched. The annealed samples were then also studied by TEM and SAXS.

To avoid heating the samples to the point where decomposition would begin, thermogravimetric analysis (TGA) was also performed on pieces of the cast and dried but unannealed PCHD homopolymer film. These experiments were carried out under dynamic N_2 flow with a ramping rate of 10 °C/min and revealed that weight loss occurs in two steps. An initial loss of 6−8 wt % was observed by 120 °C and was ascribed to residual solvent trapped inside the polymer film during the casting process. Thermally annealed samples, for which the morphology was studied, were kept under vacuum at 120 °C for over 1 week. TGA of these annealed samples showed virtually no remaining residual solvent. In TGA the majority of weight was lost beginning at about 300 °C, corresponding to degradation of PCHD.[26,27] Polystyrene is known to decompose beginning at about 350 °C. Clearly then our thermal annealing at 120 °C does not present a risk of sample degradation.

The T_g of PCHD was determined by performing differential scanning calorimetry (DSC) on cast films, of homopolymer PCHD film (M_n = 13 700 and M_w = 18 000). To erase any prior thermal history, the sample was heated from room temperature to 100 °C at a ramp rate of 10 °C/min and then quenched to −70 °C and scanned a second time under the same conditions. The T_g for the rescan was consistently measured at 22 °C. The DSC results also suggest the presence of residual casting solvent in unannealed samples. Continued rescans resulted in a steady increase in T_g as the residual solvent was lost, up to 53 °C by the fourth scan. This higher value is more consistent with reported literature values for the T_g of polycyclohexadiene homopolymers,[19] those with higher 1,2 content.

To examine the effects of casting, annealing, and fractionating on the samples, size exclusion chromatography (SEC) data were obtained for each sample using a Wyatt DAWN tandem SEC-light scattering unit with THF eluent. Separation was achieved with a series of three mixed-C columns from Polymer Laboratories, and the acquired scans were compared with those of the as-synthesized material. In particular, the six samples which formed the best core−shell cylinder morphologies (CS* in Table 3) were examined to determine whether decomposition or cross-linking had occurred. Figure 1 shows the SEC traces for a representative sample (PS−PCHD-3 cast from cyclohexane) which displayed extremely well ordered core−shell cylinder morphology in the unfractionated-annealed as well as the fractionated states. None of the samples exhibited significant decomposition or cross-linking.

All of the samples (annealed and unannealed) were cryomicrotomed using a Leica Ultramicrotome and a Diatome

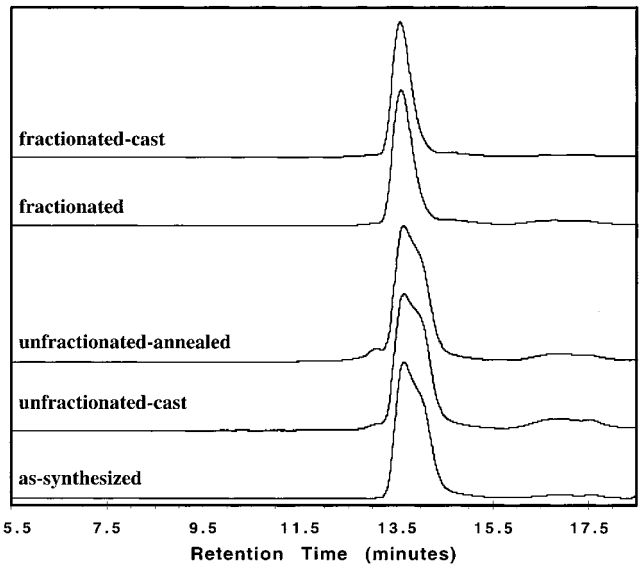

Figure 1. Composite graph of SEC traces from the various PS−PCHD-3 cyclohexane samples, offset for clarity: (a) PS−PCHD-3 polymer as-synthesized; (b) polymer after casting from cyclohexane at 25 °C; (c) polymer cast from cyclohexane and then annealed; (d) fractionated PS−PCHD-3; (e) fractionated polymer cast from cyclohexane at 25 °C.

diamond knife. Optimal conditions for microtoming were obtained with knife temperatures of −90 °C and sample temperatures of −100 °C. Slices ranging in thickness from 300 to 500 Å were collected and stained in OsO_4 vapors until the morphology was readily visible, typically 12 h. The OsO_4 attacks the double bonds in the polycyclohexadiene blocks, rendering those microphase-separated domains dark in TEM via mass thickness contrast. TEM was performed on a JEOL 100CX transmission electron microscope, operating at 100 kV accelerating voltage. Polystyrene latex sphere standards (0.091 μm diameter) were used as an internal calibration for the microscope magnification.

Small-angle X-ray scattering (SAXS) patterns were collected on beamline X27C of the National Synchrotron Light Source at Brookhaven National Laboratory. The 3 mm^2 beam had a wavelength of 1.307 Å with a camera length of 1.410 m. The 2D patterns were recorded onto Fujitsu HR-V image plates and digitized using a Fujitsu BAS 2000 scanner. Extraneous background scatter was subtracted, and the data was converted to a logarithmic scale. Circular averaging was performed to produce a plot of intensity vs scattering angle, q.

Results

Representative TEM micrographs of sample PS−PCHD-1 cast from toluene are shown in Figure 2 for both as-cast and annealed samples. In both cases a hexagonally packed lattice of core−shell cylinder domains is observed. These structures are comprised of an inner cylindrical core of PS surrounded by an annular cylinder of PCHD (stained dark in the micrographs). The core−shell structures are then embedded in a matrix of PS. Figure 2a shows a projection down the cylinder axis in which the hexagonal lattice and the PS cores in the middles of the cylinders are clearly visible. Figure 2b shows a projection normal to the cylindrical axes. As shown schematically in Figure 3, the white stripes arise from projection through the unstained PS matrix while missing the cylinders. The thin, very dark stripes result from projection through the PCHD annuli in regions where the edges of the annuli are nearly parallel to the projection direction. The gray stripes between pairs of the thin dark stripes are due to projections through the core−shell cylinder

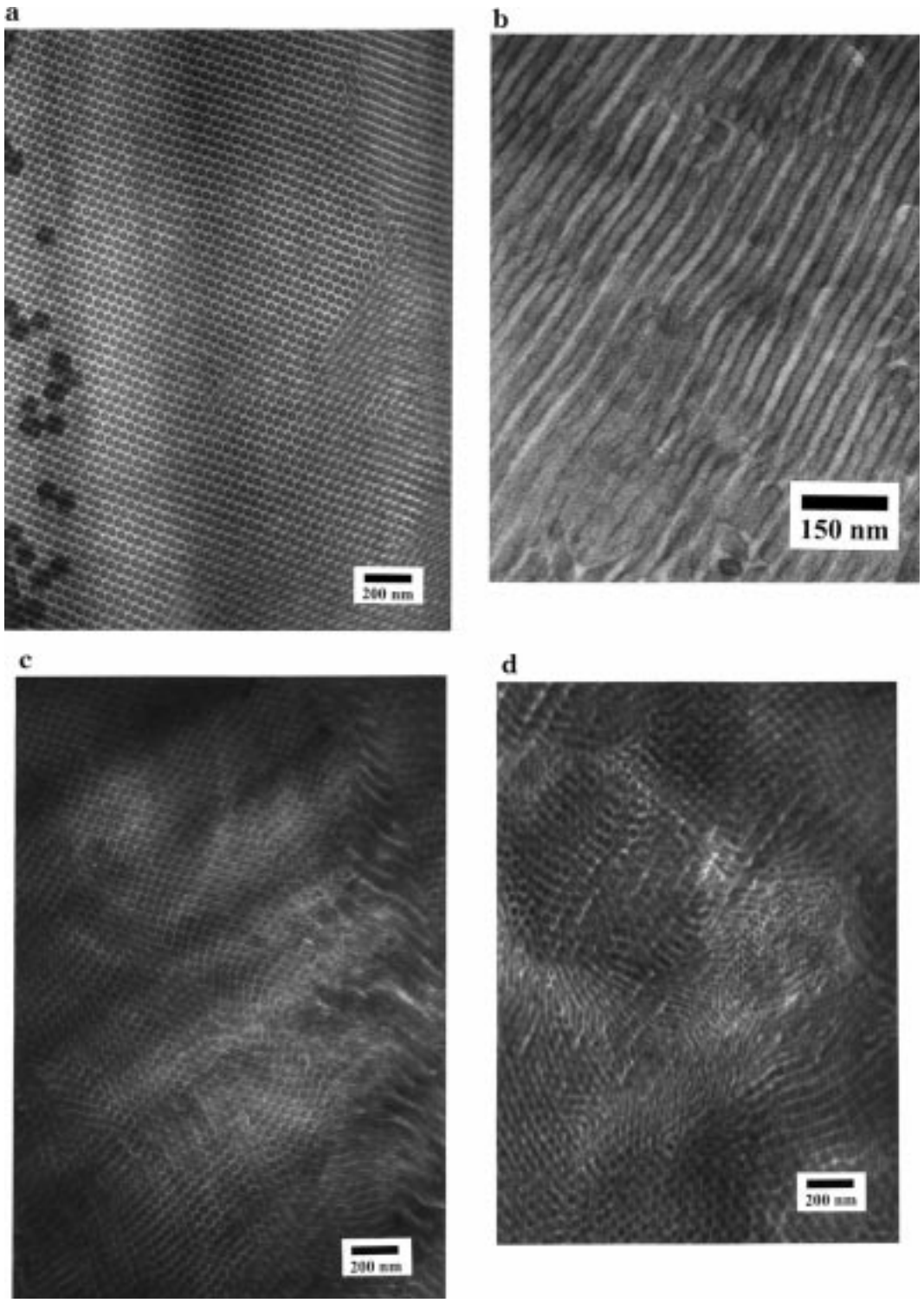

Figure 2. TEM micrographs of unfractionated PS−PCHD-1, cast from toluene: (a) projection down the cylinder axis in the unannealed sample; (b) projection perpendicular to the cylinder axis in the unannealed sample; (c) representative micrograph of the annealed sample; (d) coexistence of solid and core−shell cylinders in the annealed sample.

structures in regions where the walls of the PCHD annuli are nearly perpendicular to the projection direction. If both the stained PCHD shell material and the unstained PS core material are sampled, in the latter case, an intermediate gray level of contrast is obtained. For the annealed sample, Figure 2c shows an image which displays projections down the cylinder axis, normal to the cylinder axis, and other projections as well. Figure 2d shows an isolated region of the toluene cast PS−PCHD-1 sample after annealing, in which a small region of solid cylinders is found coexisting with the core−shell structure. This was the only such region observed for this sample; the morphology elsewhere is completely core−shell. The structural and dimensional differences between the two morphologies are clearly visible in this region of coexistence. Both the diameter of the core−shell cylinders and the intercylinder distance (lattice parameter) in the core−shell structure are significantly larger than the corresponding dimensions for the solid cylinders. The difference in solid and core−shell cylinder lattice dimensions is a clear indication that the core shell cylinder structures cannot be due to

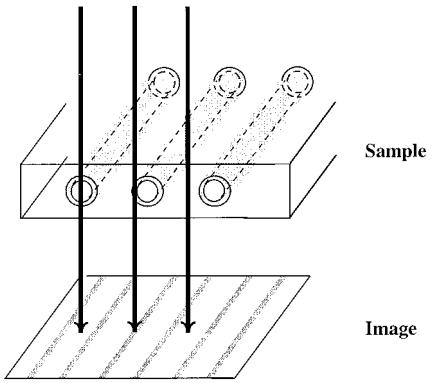

Figure 3. Schematic representation of the core−shell cylinder structure. Ray tracing arrows illustrate the origin of the light- and dark-banded morphology observed in TEM projection perpendicular to the cylinders.

a staining artifact or to Fresnel fringes produced by the microscope focus. (The core−shell cylinder structure was clearly visible across a range of focus conditions.) Such artifacts operating on solid cylinders could, perhaps, create a dark ring and may make the cylinders appear larger; however, there is no way for either artifact to substantially increase the lattice spacing.

The value of χ between PS and PCHD is not currently known, and we plan future experiments to determine this value in the temperature range of our sample annealing. On the basis of the TEM images and on the SAXS data, the structures appear to be quite strongly segregated.

Figure 4 shows TEM micrographs of PS−PCHD-1 cast from cyclohexane solution, both before and after annealing. Before annealing (Figure 4a), a morphology of conventional solid cylinders of PCHD in a PS matrix is observed. After annealing (Figure 4b), the structure is transformed into well-ordered core−shell cylinders. The scale bars confirm that the dimensions of the cylinders have been altered as a result of this transition; the radii of the core−shell cylinders are larger and the lattice parameter is about 1.5 times that of the solid cylinders. The staining conditions for both of these samples were identical and thus are not likely the cause of the morphological effects observed. Two-dimensional areas of the light and dark domains were calculated using hexagonal unit cells with the dimensions measured from the pre- and postannealed micrographs. The fractions of total light and dark areas are found to agree to within experimental error before and after annealing and to agree with the volume fractions of the samples. The details of these calculations are examined more closely in the discussion section of this paper. Thus, it appears that the annealing process has resulted in a redistribution of the PS and PCHD blocks in order to produce a new morphology.

Toluene and cyclohexane are the more selective solvents for PCHD, and casting from these solvents results in core−shell morphology and better microphase-separated order overall. Figure 5 shows the results of casting PS−PCHD-1 from THF, a solvent which is preferential for PS. Core−shell cylinders are again observed both before and after annealing, although the morphologies are less well ordered than those produced from toluene and cyclohexane. Casting from dioxane, also selective for PS, produces a disordered, chaotic morphology.

Figure 6 shows TEM images of sample PS−PCHD-3 cast from cyclohexane. Before annealing, the sample

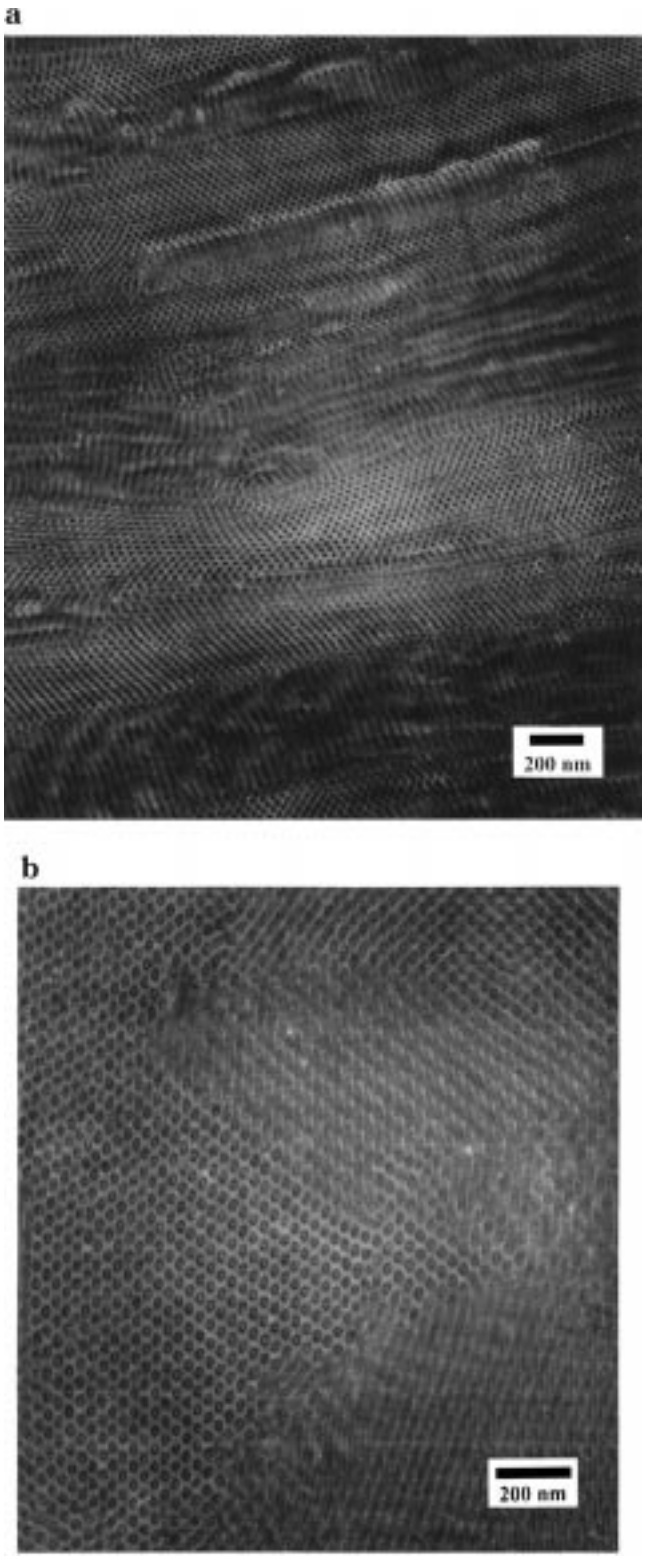

Figure 4. TEM micrographs of unfractionated PS−PCHD-1 cast from cyclohexane: (a) Solid cylinder morphology of the as-cast sample; (b) core−shell cylinder morphology obtained after annealing.

showed poorly ordered solid cylinders; projections both down the cylinder axis (Figure 6a) and normal to the cylinder axis (Figure 6b) are visible. After annealing, a well-ordered core−shell cylinder morphology is observed (Figure 6c). As was the case for the transition from solid to core−shell cylinders observed in cyclohexane cast PS−PCHD-1, in PS−PCHD-3 the area fractions of the light and dark domains (as seen in the end on projection)

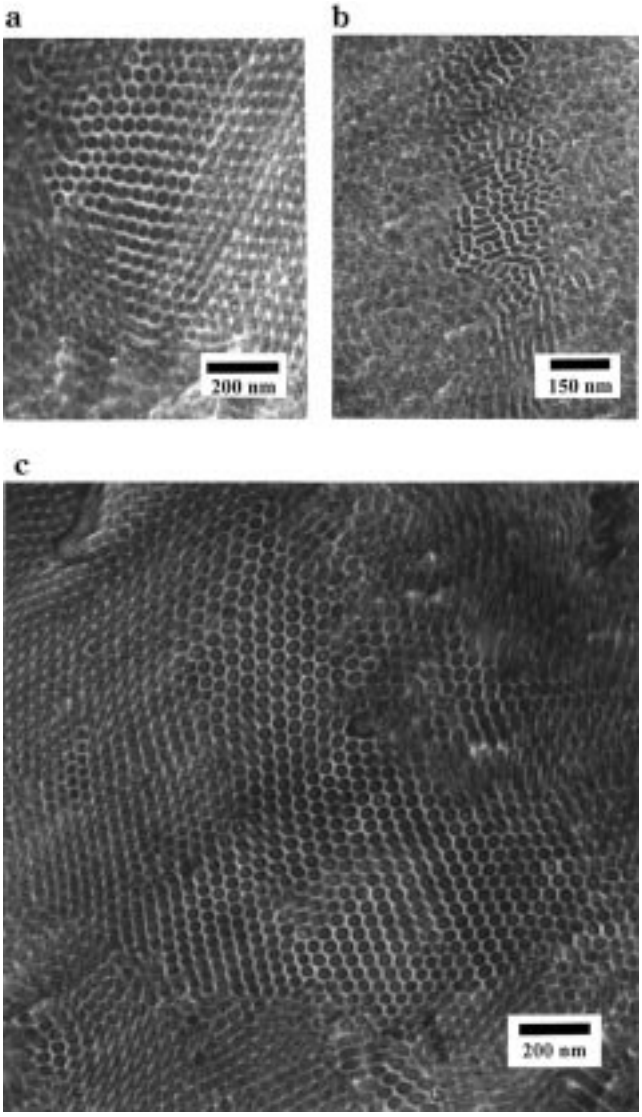

Figure 5. TEM micrographs of PS−PCHD-1 cast from THF: (a) micrograph of the unfractionated and unannealed sample showing evidence of core−shell cylinders; (b) micrograph of the unfractionated and annealed sample; (c) improved core−shell cylinder morphology of the fractionated sample.

are the same within experimental error for both the solid cylinders and core−shell cylinders. Casting from toluene produced a more poorly ordered microphase-separated structure (Figure 7a) which bears some similarity to the better ordered core−shell structures observed under other conditions. Local hexagonal packing of domains is present, and some domains appear to have a lighter spot in their centers. The order of the toluene cast PS−PCHD-3 morphology did not change noticeably upon annealing (Figure 7b). Casting PS−PCHD-3 from THF and dioxane produced even more poorly ordered morphologies. There is some indication of poorly ordered core−shell structure in the THF cast samples, but no indication of such order in those cast from dioxane. Annealing does not significantly improve the ordering of these morphologies. Here again, as with PS−PCHD-1, the solvents which are more selective for PCHD (toluene and cyclohexane) seem to promote better ordered structures. Sample PS−PCHD-2 formed core−shell structures upon casting from all four solvents used, although none of the morphologies were as well ordered as the better examples from PS−PCHD-1 and PS−PCHD-3.

After annealing, the PS−PCHD-1 sample cast from toluene produced the SAXS pattern shown in Figure 8. The presence of a number of higher order Bragg peaks is indicative of the high degree of order present in this sample. We know from the TEM micrographs that the 100 spacing of the hexagonal lattice is at least 450 Å and thus the 100 reflection is cut off by the beam stop in Figure 8. If q^* is the scattering vector of this missing primary peak and q_n is that for each succeeding reflection ($n = 1, 2, 3, ...$), then the ratios, q_n/q^* for this pattern match the ratios expected for cylinders arranged on a hexagonal lattice: $1, \sqrt{3}, \sqrt{4}, \sqrt{7}, \sqrt{9}, \sqrt{12}$ .... The lowest angle peak observed has $q_n/q^* = \sqrt{3}$. This indexing of the reflections allows the determination of the 100 spacing as 640 Å and the hexagonal lattice constant as 740 Å from the SAXS data.

PS−PCHD-1 samples cast from cyclohexane displayed a striking change in morphology from solid cylinders before annealing to core−shell cylinders after annealing. The SAXS data for the unannealed solid cylinder sample (Figure 9a) shows Bragg peaks at scattering vector ratios corresponding to cylinders ordered on a hexagonal lattice; $q_n/q^* = 1, \sqrt{3}, \sqrt{4}$, and $\sqrt{7}$. In this case, for the smaller solid cylinder lattice, the lowest angle peak observed is the 100 reflection. This scattering data indicates a 100 spacing for the solid cylinders of 360 Å and a hexagonal lattice parameter of 420 Å. After annealing, the much better ordered core−shell cylinders produced scattering (Figure 9b) with more higher order Bragg peaks: $q/q^* = \sqrt{3}, \sqrt{4}, \sqrt{7}, \sqrt{9}, \sqrt{12}$ and perhaps $\sqrt{39}$. As in Figure 8, the q^* peak is obscured by the beam stop. Fitting the observed peaks to the series of scattering vector ratios for a hexagonal lattice beginning with $\sqrt{3}$ allows the determination of the 100 d spacing as 630 Å and the hexagonal lattice parameter as 720 Å, in excellent agreement with the values from the toluene-cast sample. Thus, scattering quantifies the increase in the core shell lattice parameter relative to that of solid cylinders. This provides additional supporting evidence for the core−shell structure in material which, unlike the samples used for TEM, has not been stained.

Analysis of SAXS from the THF cast PS−PCHD-1 samples allows identification of a hexagonal packing. However, the relatively poor order of these samples makes more in-depth analysis difficult.

Sample PS−PCHD-3 cast from cyclohexane produced solid cylinders before annealing and core−shell cylinders after annealing. The log I vs q SAXS data for these samples are plotted in Figure 10a (before annealing) and Figure 10b (after annealing). The solid cylinders (Figure 10a) show Bragg peaks at ratios corresponding to cylinders ordered on a hexagonal lattice: $q_n/q^* = 1, \sqrt{3}$, and $\sqrt{7}$. The first peak in observed in this case is the 100 reflection, with a spacing of 340 Å. This corresponds to a lattice constant for the solid cylinders of 390 Å. It is difficult to tell whether the maximum expected at $\sqrt{4}$ is also present. After annealing (Figure 10b), the better ordered core−shell cylinder structure produces higher order Bragg reflections with scattering vector ratios expected for cylinders arrayed on a hexagonal lattice: $\sqrt{3}, \sqrt{4}, \sqrt{7}, \sqrt{9}, \sqrt{12}, \sqrt{16}$, and $\sqrt{21}$, and perhaps $\sqrt{28}$. As before, the q^* peak is obscured by the beam stop. Fitting the observed peaks to the series of scattering vector ratios for a hexagonal lattice begin-

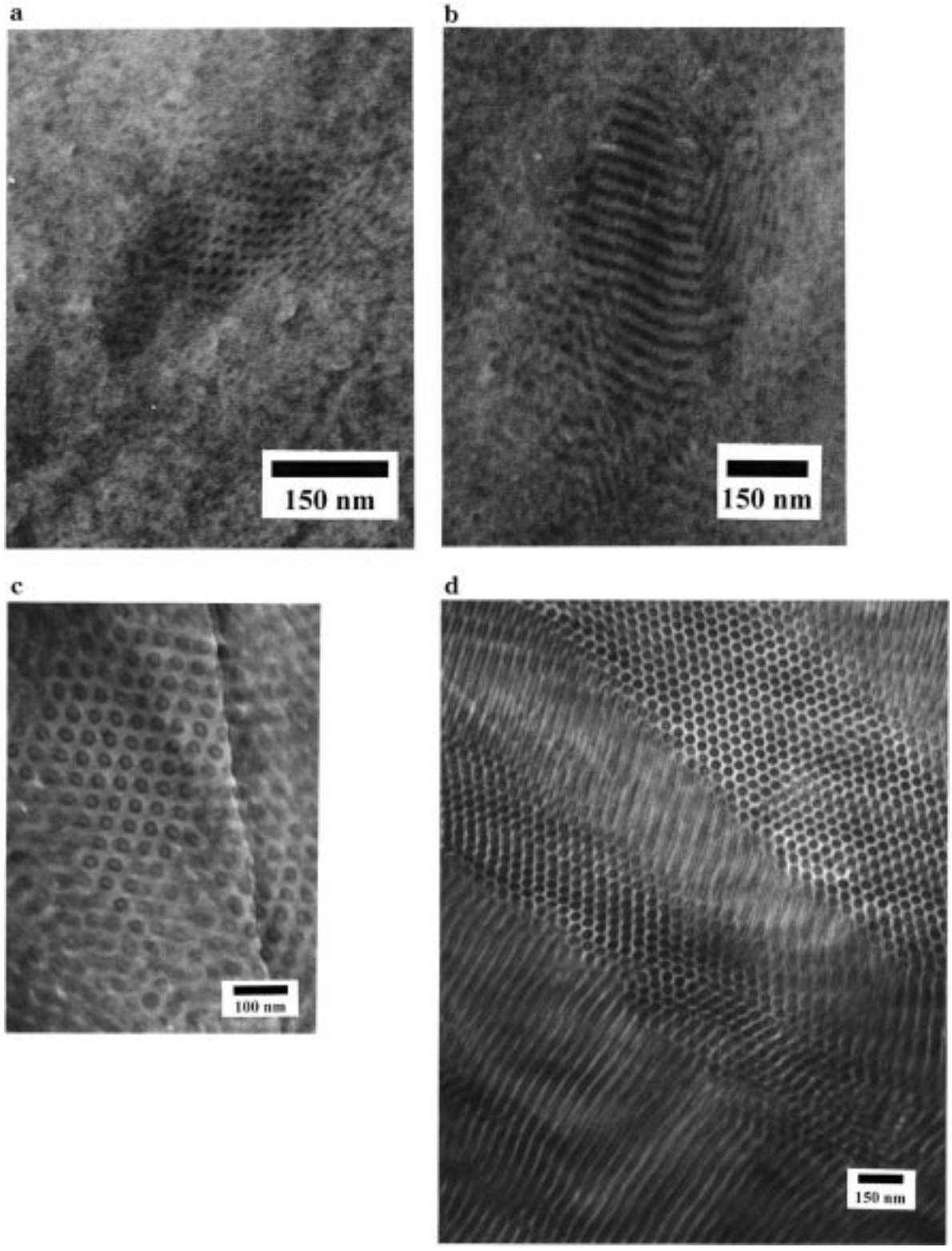

Figure 6. TEM micrographs of PS−PCHD-3 cast from cyclohexane: (a) unfractionated sample displaying solid cylinder morphology, view showing end-on projection of the cylinders; (b) unfractionated sample, projection normal to solid cylinder axes; (c) unfractionated, annealed sample showing well-ordered core−shell cylinders; (d) fractionated sample showing highly ordered core−shell morphology.

ning with $\sqrt{3}$ allows the determination of the 100 *d* spacing as 600 Å and the hexagonal lattice parameter as 700 Å.

SEC data revealed that all three as-synthesized samples (PS−PCHD-1, PS−PCHD-2, and PS−PCHD-3) contained significant amounts of polystyrene homopolymer and a very small amount of PCHD homopolymer. The shoulders at longer retention times than the main peaks, shown for the case of PS−PCHD-3 in Figure 1, correspond to the exact molecular weight of the polystyrene block in PS−PCHD-3. (The PS block was sampled before addition of CHD monomer and characterized by SEC.) Similar SEC traces were obtained for PS−PCHD-1 and PS−PCHD-2. This ho-

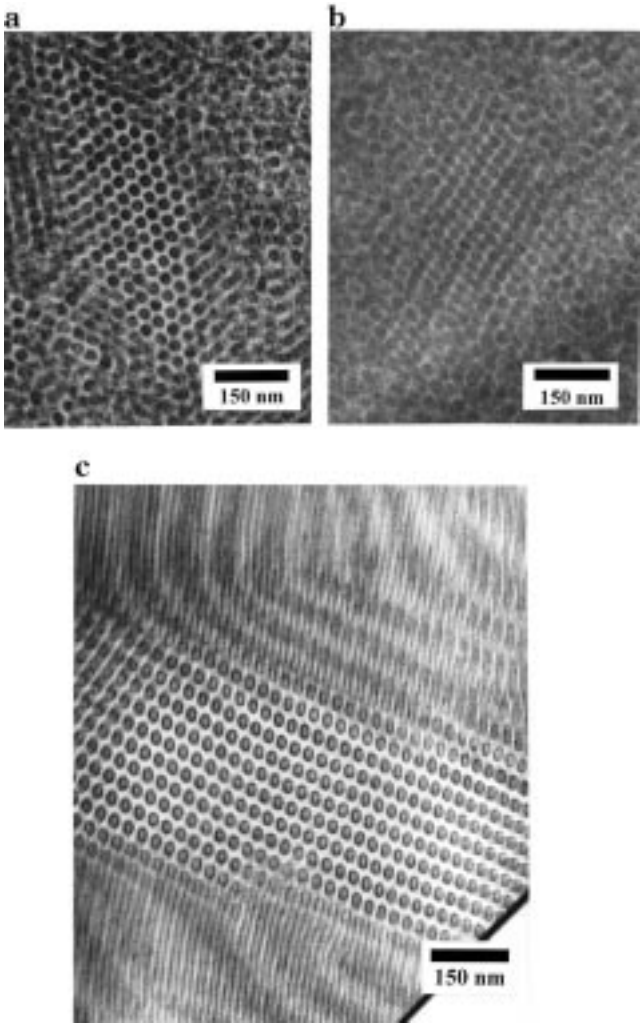

Figure 7. TEM micrographs of PS−PCHD-3 cast from toluene: (a) poorly ordered core−shell microphase-separated structure of the unfractionated and unannealed sample; (b) poorly ordered core−shell microphase-separated structure of the unfractionated, annealed sample; (c) well-ordered core−shell cylinder morphology observed in the fractionated and annealed sample.

mopolymer contamination is attributed to incomplete crossover from styrene to cyclohexadiene during the synthesis of the diblocks. To understand the effect that polystyrene homopolymer has upon the unique core−shell cylinder microphase-separated morphology, the as-synthesized samples PS−PCHD-1 and PS−PCHD-3 were fractionated several times to remove the polystyrene. The SEC chromatograms and MALDI−TOF−MS spectra for PS−PCHD-1 and PS−PCHD-3 after fractionation indicate effective removal of the homopolymer impurity, as is shown for PS−PCHD-3 in Figure 1. Fractionated polymers of PS−PCHD-1 and PS−PCHD-3 were then cast from the four solvents used previously, and the morphologies of the unannealed and annealed films were examined using TEM and SAXS.

The pure PS−PCHD diblock copolymer, resulting from fractionation to remove homopolymer, showed an enhancement in regularity and long range order of core−shell cylinder morphology. Figure 5c shows the very well ordered core−shell cylinder structure formed when fractionated PS−PCHD-1 is cast from THF. This structure is much more perfect than those shown in parts a and b of Figure 5 for the unfractionated material cast from THF. Figure 6d shows the excellent core−shell

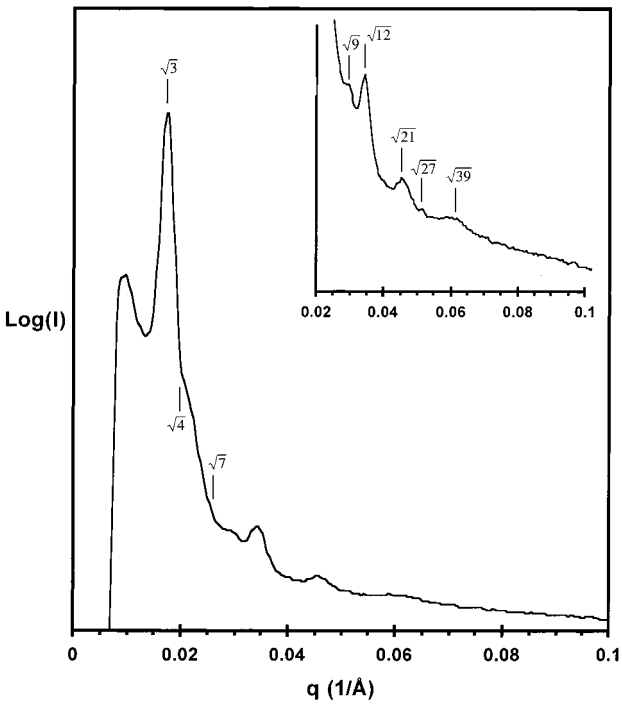

Figure 8. SAXS data for unfractionated, annealed PS−PCHD-1 cast from toluene. Scattering vector ratios for reflections are indicated.

cylinder structure obtained by casting fractionated PS−PCHD-3 from cyclohexane. This structure is also considerably more well ordered than unfractionated PS−PCHD-3 cast under the same conditions. Figure 7c shows projections down the cylinder axis and normal to the cylinder axis of a very well ordered core−shell structure obtained by casting fractionated PS−PCHD-3 from toluene and then annealing. The unannealed, fractionated PS−PCHD-3 cast from toluene also shows excellent core−shell order, similar to Figure 7c. Before fractionation, casting PS−PCHD-3 from toluene produced a poorly ordered morphology, which was barely recognizable as core−shell. SAXS of toluene cast and annealed PS−PCHD-3 is shown in Figure 11. The excellent core−shell cylinders with hexagonal long range order leads to Bragg peaks with scattering vector ratios of $q/q^* = \sqrt{3}, \sqrt{4}, \sqrt{7}, \sqrt{9}, \sqrt{12}, \sqrt{21}$, and $\sqrt{39}$. Again, the 100 reflection is obscured by the beam stop.

The results of the TEM imaging and SAXS studies on the as-cast and annealed samples are summarized in Table 3, along with the results from the fractionated diblock materials. As shown in the table, samples which exhibit the best core−shell cylinder morphologies are those cast from solvents selective for the polycyclohexadiene (cyclohexane and toluene).

Discussion

Table 4 lists volume fractions calculated for different components of the core−shell morphology, based on SAXS data and on measurements taken from TEM micrographs. In the table, these values are compared to volume fractions calculated based on the molecular characterization of the as-synthesized and fractionated PS−PCHD-1 and PS−PCHD-3 materials. Since the OsO_4 staining procedure, microtoming stresses, and projection artifacts in TEM can all act to distort dimensions measured on the micrographs from true values characteristic of the structure, the measured dimen-

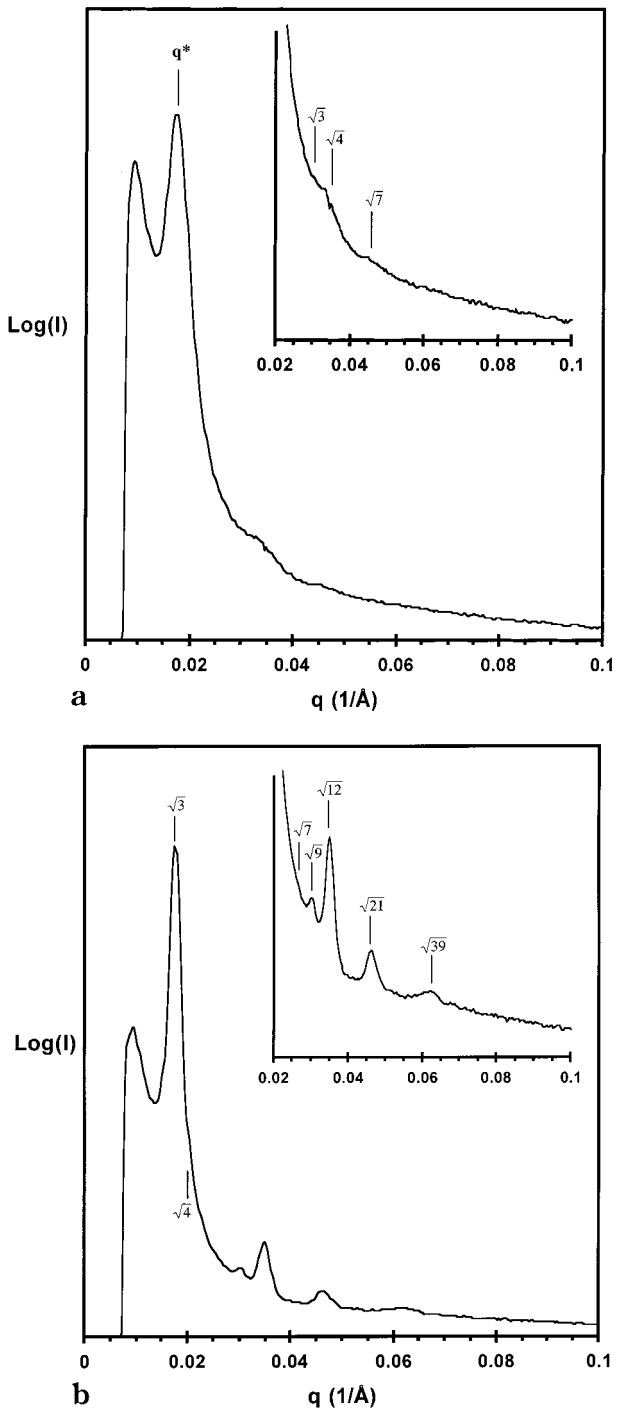

Figure 9. SAXS data for unfractionated PS−PCHD-1 cast from cyclohexane with scattering vector ratios of reflections as indicated: (a) data from the unannealed sample; (b) annealed sample experimental SAXS.

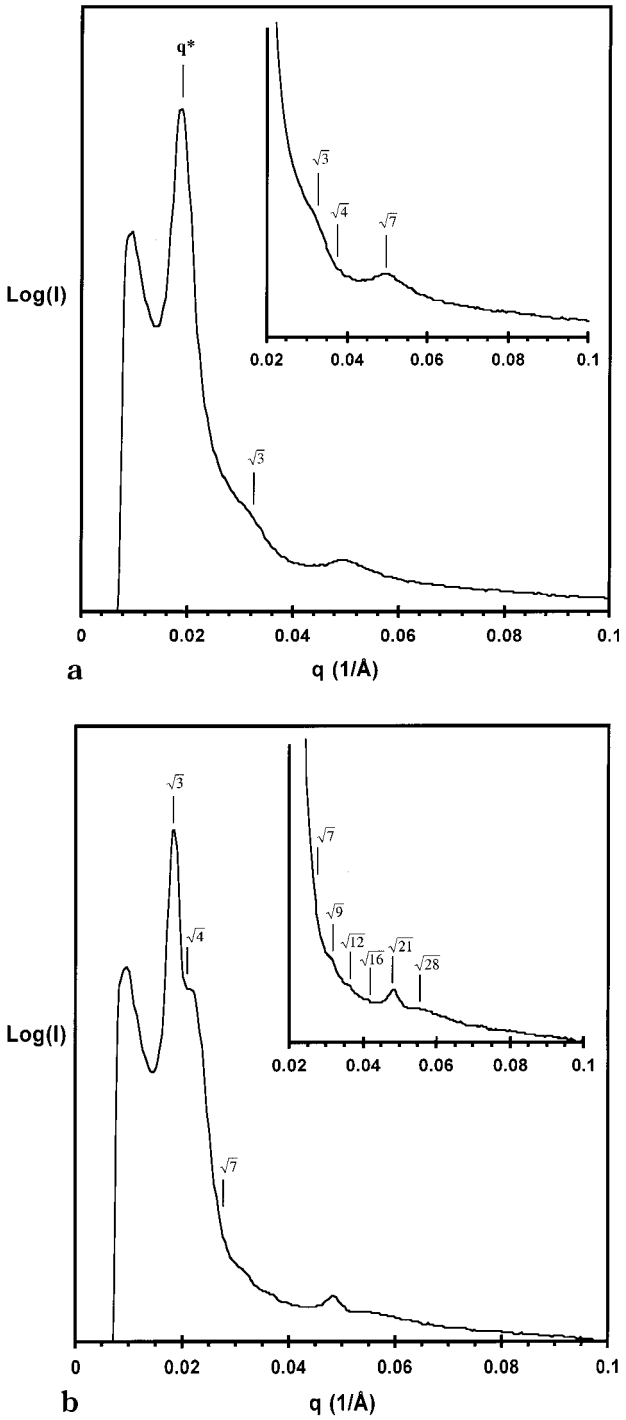

Figure 10. SAXS data for unfractionated PS−PCHD-3 cast from cyclohexane with scattering vector ratios of reflections as indicated: (a) data from the unannealed sample; (b) Annealed sample experimental SAXS.

sions, and thus the calculated volume fractions, may contain substantial error. Thus, only qualitative comparisons can be made, the purposes of which are to verify general trends expected for the core−shell cylinder morphology.

The volume fractions calculated for the PCHD domains, based on TEM images, agree quite well with the values based on NMR. For both PS−PCHD-1 and PS−PCHD-3 there is an increase in the PCHD volume fraction from the as-synthesized material to the fractionated material, which is as expected since PS homopolymer has been removed from these samples. This increase in PCHD volume fraction is found in both the values calculated from TEM micrographs and those calculated from NMR. Volume fractions based on measurements from TEM images were also calculated for the total material in the cylinder domains (the sum of the core and shell.) These total cylinder volume fractions are substantially larger in all cases than the PCHD volume fractions calculated either from TEM or from NMR. This is significant since it indicates that the structures must have PS in their centers in order to conserve volume. The fact that the core−shell cylinders are larger than conventional solid cylinder diblock

Table 4. Cylinder Calculations

	core−shell cylinders				solid cylinders	
	PS−PCHD-1 cast/ann	PS−PCHD-1 fract	PS−PCHD-3 cast/ann	PS−PCHD-3 fract	PS−PCHD-1 cast	PS−PCHD-3 cast
outer diameter (nm)[a]	33	31	31	24	21	16
inner diameter (nm)[a]	20	18	17	11		
TEM $d(100)$ (nm)[a]	41	37	39	28	32	27
SAXS $d(100)$ (nm)	63	49	60	61	36	34
ϕ (entire cylinder)[b]	0.44[d]	0.47[d]	0.42[d]	0.48[d]	0.30[e]	0.23[e]
ϕ (cylinder core)[b] (unstained PS)	0.17	0.17	0.12	0.11		
ϕ (cylinder annulus)[b] (stained PCHD)	0.27	0.30	0.30	0.38		
calcd ϕ (PCHD)[c]	0.34	0.37	0.30	0.38	0.34	0.30
fraction of PS chains facing into core		0.24		0.18		

[a] Measured directly from the micrographs. [b] Calculated using the measured diameters and $d(100)$ spacings from the micrographs. [c] Calculated by integration of the 600 MHz ^{1}H NMR spectrum (see Table 1). [d] The "entire cylinder" is comprised of both the unstained PS core and the stained PCHD annulus. [e] In this case the "entire cylinder" is simply the solid, stained PCHD cylinder.

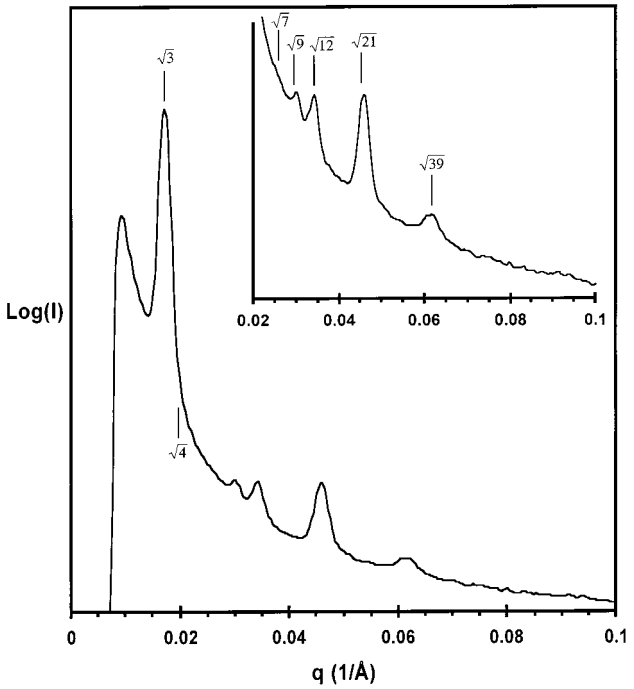

Figure 11. SAXS data for fractionated PS−PCHD-3 cast from toluene and annealed.

copolymer morphologies is evident from the TEM images of this structure; these show that the cylindrical domains are separated by less matrix material than one sees with conventional cylinder morphologies. In the case of the fractionated PS−PCHD-1 and PS−PCHD-3 samples, the volume fractions of the core−shell cylinder structures are 0.47 and 0.48, respectively. These values are considerably higher than the volume fraction range in which one expects to see conventional cylinders in diblocks. In Figure 2d, which shows coexisting solid and core−shell cylinders, a direct comparison of the cylinder sizes is possible. It seems plausible, based on this image, that the volume fraction of PCHD in the solid cylinders is the same as that in the annuli of the core−shell cylinders. This assertion has been checked by measuring the solid cylinder dimensions in the unannealed PS−PCHD-1 and PS−PCHD-3 samples cast from cyclohexane and comparing these preannealed cylinder volume fractions with those of the PCHD annuli in the corresponding core−shell cylinder structures which developed after annealing. As shown in Table 4, there is reasonable agreement (considering the approximate nature of calculations based on measurements from TEM images) between the PCHD volume fractions of the solid cylinder and core−shell morphologies. They differ by only 0.03 and 0.07 for PS−PCHD-1 and PS−PCHD-3, respectively. The volume fractions of the PS material found in the cylindrical core regions, calculated from measurements on TEM micrographs, range from 0.11 to 0.17. This is within the range of volume fractions for which spherical domains would normally be expected. The volume fractions of the PCHD blocks, as measured by ^{1}H NMR for the fractionated samples (0.37 and 0.38), places these polymers within the narrow range where the cubic bicontinuous gyroid microstructure has been previously observed for diblock copolymer systems.[2,3,10] The TEM projections observed and the clear hexagonal symmetry of the SAXS data prove that this material does not form a gyroid structure.

The proposed core−shell structure requires that the junction points between the PCHD and PS blocks lie on both the inner and outer surfaces of the PCHD annular domains; some diblocks must have their PS blocks facing out, into the matrix, while others must face into the core. By comparison of the relative volumes of PS core material and PS matrix material from TEM micrographs of the fractionated samples, it is found that about 20% (24% for PS−PCHD-1 and 18% for PS−PCHD-3) of the chains are pointing into the core and 80% are facing out.

In the analysis of a core−shell cylinder morphology in an ABC triblock, Gido, Thomas, and co-workers[17] showed that the outer interface between the annular domain and the matrix is pushed out, close to the boundary of the Wigner−Seitz cell surrounding each cylindrical element. When this happens, the interface will deviate from a constant mean curvature (rounded) geometry and, instead, develop a hexagonal shape with sharp edges. In the present study, the core−shell structure does lead to larger cylindrical elements, pushing the outer interface closer to the boundary of the Wigner−Seitz cell. However, no deviation from constant mean curvature is detectable in these PS−PCHD structures. This is understandable based on the calculated interface shapes presented in the Gido and Thomas paper. The interface does not begin to deviate noticeably from constant mean curvature until the volume fraction of the matrix material drops below about 0.4. The lowest PS matrix volume fractions in this study were 0.53 and 0.52 in the fractionated PS−PCHD-1 and PS−PCHD-3 samples.

Conclusions

The TEM and SAXS results of this study clearly demonstrate the formation of a core−shell cylinder morphology in PS−PCHD diblock copolymers and blends of these diblocks with homopolystyrene. However, we cannot state conclusively that this new structure is an equilibrium morphology. Certainly, the formation of this structure does seem to depend on the use of the correct casting solvent. Cyclohexane and toluene produce the best core−shell structures, THF produces less well-ordered structures, and dioxane produces chaotic disordered structures. Annealing can increase the order of the core−shell structures, and this would seem to point toward the stability of the structure. However, annealing was not able to produce core−shell order from the disordered dioxane cast samples. Physically it seems strange that an equilibrium structure would result in such a large difference in the physical environment of identical diblock chains, with some pointing in toward the core and others pointing out toward the matrix. Recent preliminary calculations indicate that the core−shell structure in PS−PCHD diblocks may represent an energetic local minimum.[28] If the structure is metastable, this could explain the reproducibility of our results and the fact that the order can be improved by thermal annealing. It would also explain why some sample preparation routes do not lead to the structure even after annealing.

To determine conclusively whether the core−shell structure is a local or a global energy minimum, values of χ between PS and PCHD and the statistical segment length of PCHD must be determined, as they are not currently available for this system. At present we are conducting experiments to accurately determine these parameters.

Acknowledgment. The authors thank Dr. Philipp Janert for performing preliminary calculations as well as for helpful discussions. We are also grateful to Dr. Darrin Pochan for the initial work he did on these samples. This research was funded by the U.S. Army Research Office under Contracts DAAG55-98-1-0116 and DAAG55-98-1-0005. Central Facility support from the Materials Research Science and Engineering Center (MRSEC) at the University of Massachusetts-Amherst, as well as the W. M. Keck Electron Microscopy Laboratory are also acknowledged.

References and Notes

(1) Thomas, E. L.; Alward, D. B.; Kinning, D. J.; Martin, D. C.; Handlin, D. L., Jr.; Fetters, L. J. *Macromolecules* **1986**, *19*, 2197.
(2) Hasegawa, H.; Tanaka, H.; Yamasaki, K.; Hashimoto, T. *Macromolecules* **1987**, *20*, 1651.
(3) Hajduk, D. A.; Harper, P. E.; Gruner, S. M.; Honeker, C. C.; Kim, G.; Thomas, E. L.; Fetters, L. J. *Macromolecules* **1994**, *27*, 4063.
(4) Schulz, M. F.; Bates, F. S.; Almdal, K.; Mortensen, K. *Phys. Rev. Lett.* **1994**, *73*, 86.
(5) Hajduk, D. A.; Harper, P. E.; Gruner, S. M.; Honeker, C. C.; Thomas, E. L.; Fetters, L. J. *Macromolecules* **1995**, *28*, 2570.
(6) Avgeropoulos, A.; Dair, B. J.; Hadjicristidis, N.; Thomas, E. L. *Macromolecules* **1997**, *30*, 5634.
(7) Hashimoto, T.; Koizumi, S.; Hasegawa, H.; Izumitani, T.; Hyde, S. T. *Macromolecules* **1992**, *25*, 1433.
(8) Disko, M. M.; Liang, K. S.; Behal, S. K.; Roe, R. J.; Jeon, K. J. *Macromolecules* **1993**, *26*, 2983.
(9) Hamley, I. W.; Koppi, K. A.; Rosedale, J. H.; Bates, F. S.; Almdal, K.; Mortensen, K. *Macromolecules* **1993**, *26*, 5959.
(10) Förster, S.; Khandpur, A. K.; Zhao, J.; Bates, F. S.; Hamley, I. W.; Ryan, A. J.; Bras, W. *Macromolecules* **1994**, *27*, 6922.
(11) Mogi, Y.; Nomura, M.; Kotsuji, H.; Ohnishi, K.; Matsushita, Y.; Noda, I. *Macromolecules* **1994**, *27*, 6755.
(12) Stadler, R.; Auschra, C.; Beckmann, J.; Krappe, U.; Voigt-Martin, I.; Leibler, L. *Macromolecules* **1995**, *28*, 3080.
(13) Breiner, U.; Krappe, U.; Abetz, V.; Stadler, R. *Macromol. Chem. Phys.* **1997**, *198*, 1051.
(14) Breiner, U.; Krappe, U.; Jakob, T.; Abetz, V.; Stadler, R. *Polym. Bull.* **1998**, *40*, 219.
(15) Breiner, U.; Krappe, U.; Thomas, E. L.; Stadler, R. *Macromolecules* **1998**, *31*, 135.
(16) Birshtein, T. M.; Lyatskaya, Y. V.; Zhulina, E. B. *Polymer* **1992**, *33*, 2750.
(17) Gido, S. P.; Schwark, D. W.; Thomas, E. L.; do Carmo Gonçalves, M. *Macromolecules* **1993**, *26*, 2636.
(18) Kipp, B. E.; Pochan, D. J.; Gido, S. P.; DeSimone, J. M. Submitted for publication in *Macromolecules.*
(19) Natori, I.; Imaizumi, K.; Yamagishi, H.; Kazunori, M. *J. Polym. Sci. B: Polym. Phys.* **1998**, *36*, 1657.
(20) François, B.; Zhong, X. F. *Makromol. Chem.* **1990**, *191*, 2743.
(21) Small, P. A. *J. Appl. Chem.* **1953**, *3*, 71.
(22) Hoy, K. L. *J. Paint Technology* **1970**, *42*, 76.
(23) Burrell, H. In *Polymer Handbook*; 2nd ed.; Brandrup, J., Immergut, E. H., Eds.; John Wiley & Sons: New York, 1975; p IV337.
(24) Krause, S. In *Polymer Blends*; Paul, D. R.; Newman, S., Ed.; Academic Press: New York, 1978; Vol. 1; p 15.
(25) Barton, A. F. M. *CRC Handbook of Solubility Parameters and other Cohesion Parameters;* 2nd ed.; CRC Press Inc.: Boca Raton, FL 1991.
(26) Zhong, X. F.; François, B. *Makromol. Chem.* **1991**, *192*, 2277.
(27) Zhong, X. F.; François, B. *Makromol. Chem. Rapid Commun.* **1988**, *9*, 411.
(28) Janert, P. K. private communication.

MA9810722